Cell, Vol. 91, 695–704, November 28, 1997, Copyright ©1997 by Cell Press

Crystal Structure at 1.7 Å Resolution of VEGF in Complex with Domain 2 of the Flt-1 Receptor

Christian Wiesmann,* Germaine Fuh,*
Hans W. Christinger, Charles Eigenbrot,
James A. Wells, and Abraham M. de Vos†
Genentech, Inc.
Department of Protein Engineering
South San Francisco, California 94080

Summary

Vascular endothelial growth factor (VEGF) is a homodimeric hormone that induces proliferation of endothelial cells through binding to the kinase domain receptor and the Fms-like tyrosine kinase receptor (Flt-1), the extracellular portions of which consist of seven immunoglobulin domains. We show that the second and third domains of Flt-1 are necessary and sufficient for binding VEGF with near-native affinity, and that domain 2 alone binds only 60-fold less tightly than wild-type. The crystal structure of the complex between VEGF and the second domain of Flt-1 shows domain 2 in a predominantly hydrophobic interaction with the "poles" of the VEGF dimer. Based on this structure and on mutational data, we present a model of VEGF bound to the first four domains of Flt-1.

Introduction

Vascular endothelial growth factor (VEGF) is a mitogen that is highly specific for vascular endothelial cells (Dvorak et al., 1995). As a potent angiogenic factor, it is involved in the development of the vascular system and in the differentiation of endothelial cells (Carmeliet et al., 1996; Ferrara et al., 1996). Angiogenesis is not only important in the physiological processes of embryogenesis and wound healing (Peters et al., 1993), but is also involved in pathological processes such as tumor growth, metastasis, diabetic retinopathy, and rheumatoid arthritis (Ferrara, 1995). Antibodies against VEGF can suppress tumor growth in vivo (Kim et al., 1993), indicating that VEGF antagonists could have broad therapeutic applications.

The biological function of VEGF is mediated through binding to two receptor tyrosine kinases, the kinase domain receptor (KDR; murine flk-1) and the Fms-like tyrosine kinase (Flt-1), which are localized on the cell surface of various endothelial cell types (Vaisman et al., 1990). Studies in mice have shown that the expression of KDR reaches the highest levels during embryonic vasculogenesis and angiogenesis (Millauer et al., 1993). In contrast, only low levels of mRNA for Flt-1 were found during fetal growth and moderate levels during organogenesis, but high levels in newborn mice (Peters et al., 1993). Experiments with knockout mice deficient in either receptor revealed that KDR is essential for the development of endothelial cells, whereas Flt-1 is necessary for the organization of embryonic vasculature (Fong et al., 1995; Shalaby et al., 1995).

KDR and Flt-1, together with the related receptor Flt-4, constitute a subgroup of the platelet-derived growth factor (PDGF) receptor family (Van der Greer and Hunter, 1994). Flt-1 binds VEGF in the pM range and has a 10-fold higher affinity for VEGF than KDR, while Flt-4 does not bind VEGF (Davis-Smyth et al., 1996). In addition to the VEGF receptor subgroup and the PDGF α and β receptors, the PDGF receptor family includes Fms (the macrophage colony-stimulating factor receptor) and Kit (the stem cell factor receptor). The extracellular portion of these receptors is comprised of a number of immunoglobulin domains, 7 for the VEGF subgroup and 5 for the other members. Domain deletion studies on Flt-1 (Davis-Smyth et al., 1996; Barleon et al., 1997; Cunningham et al., 1997), the PDGF receptors (Mahadevan et al., 1995), and Kit (Blechman et al., 1995; Lemmon et al., 1997) have shown that the ligand binding function resides within the first three domains. Deletion experiments on KDR show that only domains 2 and 3 are critical for ligand binding, and that domains 4–7 are not essential for signaling (Fuh et al., submitted). In addition, it has been suggested for Flt-1 (Barleon et al., 1997) and Kit (Blechman et al., 1995) that domain 4 may be required to efficiently couple ligand binding to signal transduction by means of direct receptor–receptor contacts.

VEGF is a homodimeric glycoprotein encoded by a single gene that is expressed in four different isoforms ($VEGF_{121}$, $VEGF_{165}$, $VEGF_{189}$, and $VEGF_{206}$) due to different splicing events (Houck, et al., 1991; Tischer et al., 1991), $VEGF_{165}$ being most abundant. The three longest isoforms bind heparin and are found in complex with heparan sulfate–containing proteoglycans in the extracellular matrix (Houck et al., 1991). $VEGF_{165}$ can be cleaved by plasmin to yield an N-terminal fragment consisting of residues 1–110 (Keyt et al., 1996a). This domain binds KDR and Flt-1 as tightly as $VEGF_{165}$ in the absence of heparin, but like $VEGF_{121}$ has a 100-fold decreased endothelial cell mitogenic activity (Keyt et al., 1996a). The three-dimensional structure of the receptor-binding domain of VEGF (residues 8–109) showed that it is a member of the cystine-knot growth factor superfamily (Sun and Davies, 1995), with greatest similarity to PDGF (Muller et al., 1997a, 1997b). The receptor-binding face of VEGF has been identified by mutagenesis studies (Muller et al., 1997a), revealing that the binding epitope for KDR contains two "hot spots," each of which extends across the dimer interface. Charge-reversal mutagenesis has indicated that some of these same residues are also important for VEGF binding to Flt-1 (Keyt et al., 1996b).

Here, we report the results of our domain deletion study of the extracellular portion of Flt-1, as well as the crystal structure to 1.7 Å resolution of the complex between the receptor-binding domain of VEGF ($VEGF_{8–109}$) and Flt-1 domain 2 ($Flt\text{-}1_{D2}$). We show that an Flt-1 construct consisting of domains 2 and 3 binds to VEGF with

*C. W. and G. F. are first authors on the structure determination and on the expression and domain deletion studies, respectively.
† To whom correspondence should be addressed.

Table 1. Deletion Analysis of Flt-1

	Relative K_d[a]	EC_{50} (nM)[b]			
	$VEGF_{8-109}$	MAFL1	MAFL6	MAFL8	MAFL3
Dimeric constructs					
1–7-IgG	1 (12 pM)	0.23	0.70	0.25	
1–5-IgG	1.0		0.35		
1–4-IgG	2.6	0.43	0.31	0.89	0.41
1–3-IgG	2.2	0.58	0.44	0.67	0.30
1–2-IgG	49.0	0.36	0.33	0.61	
2–3-IgG	4.5	0.38	0.46	1.33	ND[c]
Monomeric constructs					
Domains 1–7	1.9	0.68	2.69		
Domains 1–3	6.7	0.46	0.63		
Domain 2	113	4.34	2.02	33.5	

[a] Binding affinities were measured as described in the Experimental Procedures. The relative affinity was derived from averaging three independent measurements with standard errors of ±15%–25%.
[b] The EC_{50} is the half-maximally effective concentration of MAb for binding to the receptor deletion construct.
[c] ND, not detectable. These data define the binding epitope for MAFL3 to be domain one.

near wild-type affinity, and that domain 2 by itself binds VEGF only about 60-fold weaker than the entire extracellular portion. The crystal structure of the complex is the first example of a cystine-knot growth factor bound to a domain of its receptor. VEGF uses its receptor-binding face to bind Flt-1_{D2} in a predominantly hydrophobic interaction. Flt-1_{D2} has several unique features compared to other domains of the immunoglobulin superfamily (IgSF), including the other domains of its own extracellular portion; these features are probably conserved in the second domain of other members of the PDGF receptor family. We propose a model of VEGF in complex with domains 1–4 of its receptor that may be a general example of how receptors of the PDGF family bind their ligands.

Results

Determination of Minimal VEGF-Binding Fragments

Systematic carboxy-terminal deletions of the seven IgSF domains of Flt-1 were carried out to define the minimal domain(s) sufficient for high-affinity binding to VEGF. The deletion variants were first expressed in mammalian cells as proteins fused to the Fc portion of IgG (Fuh et al., submitted). The domain borders were chosen based on homology to other IgSF members (Williams and Barclay, 1988; Finnerty et al., 1993). The proper folding of all variants was verified by their ability to bind several anti-Flt-1 monoclonal antibodies (partly shown in Table 1), three of which entirely (MAFL6) or partially (MAFL1 and -8) block ligand binding. The deletions caused very little change in binding to $VEGF_{8-109}$, until domain 3 was removed from the 1–3 construct, which resulted in a 20-fold reduction in affinity (Table 1). Deletion of domain 1 did not affect binding significantly (Table 1). To test the magnitude of possible avidity effects, monomeric glycosylated versions were produced from IgG fusions of domains 1–7 and 1–3 that contained an engineered protease site. The monomeric constructs bound about 2-fold more weakly than the corresponding dimeric IgG fusions (Table 1). Thus, for Flt-1 the increase in affinity caused by the dimeric nature of the fusion constructs is only slight.

Given the ability of the constructs of domains 1–2 and 2–3 to bind VEGF tightly, the affinity of domain 2 alone (residues 129–229) for $VEGF_{8-109}$ was tested. Nonglycosylated domain 2 (Flt-1_{D2}) was produced from E. coli and found to bind with an affinity of 1 nM, or about 60-fold more weakly than the monomeric version of the entire ectodomain of Flt-1 (Table 1). This difference in affinity is approximately the same as that between the IgG fusions of domains 1–2 and 1–7, showing that glycosylation is not important for binding. Competition for native ligand between Flt-1_{D2} and intact receptors was demonstrated by the ability of Flt-1_{D2} to inhibit $VEGF_{165}$-stimulated proliferation of human umbilical vein endothelial cells with an IC_{50} of about 180 nM (Figure 1). This IC_{50} is 300-fold higher than the IC_{50} for the dimeric IgG fusion of the entire extracellular portion, in good agreement with the 110-fold lower binding constant (Table 1).

Structure Determination

Crystallization of the complex between $VEGF_{8-109}$ and Flt-1_{D2} yielded two crystal forms, diffracting to 1.7 Å and 2.7 Å, respectively (Table 2). These crystal forms contained 1 and 2 dimeric complexes per asymmetric

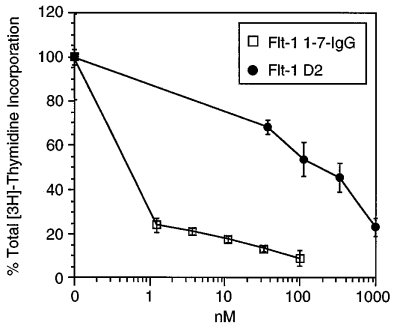

Figure 1. Inhibition of $VEGF_{165}$-Induced Growth of Human Umbilical Vein Endothelial Cells by Flt-1 Constructs

Cells were incubated for 24 hr with 0.2 nM $VEGF_{165}$ plus increasing concentrations of Flt-1_{D2} (closed circles) or the dimeric IgG fusion of domains 1–7 (open squares) and pulsed with 0.5 μCi of [^{3}H]thymidine for 18 hr before harvesting.

Table 2. Crystallization, Data Collection, and Refinement Statistics

Data Collection		
Crystal Form	A	B
Resolution (Å)	30-1.7 (1.76–1.70)[b]	30-2.7 (2.76–2.70)[b]
R_{sym} (%)[a]	5.2 (27.7)[b]	4.9 (31.1)[b]
Number of observations	332877	157478
Unique reflections	47047 (4520)[b]	24098 (1544)[b]
Completeness (%)	99.0 (95.8)[b]	99.5 (98.0)[b]
Refinement		
Resolution (Å)	20–1.7	
Number of reflections	45678	
Final R, R_{free} ($F > 0.2\sigma$)	0.199, 0.261	
Number of residues	382	
Number of water molecules	476	
Number of non-H atoms	3566	
Average B factor (Å^2)	31.9	
Rmsd bonds (Å)	0.013	
Rmsd angles (°)	1.76	
Rms ΔB for bonded atoms (Å^2)	3.7	

[a] $R_{sym} = \Sigma|I - <I>| / \Sigma I$. The summation is over all unique reflections, I is the observed intensity, and $<I>$ is the average intensity of symmetry-related observations of a unique reflection.
[b] Numbers in parentheses refer to highest resolution shell.

unit, respectively, allowing us to make extensive use of noncrystallographic symmetry averaging. The high-resolution crystal structure was refined to an R value of 19.9% (R_{free} = 26.1%), using all reflections with F greater than 0.2σ between 20 and 1.7 Å resolution (Table 2). All nonglycine residues have their main-chain torsion angles in the "most favorable" or in the "additionally allowed" regions (Laskowski et al., 1993) of the Ramachandran plot. The refined model consists of residues 13–107 and 12–109 of the two $VEGF_{8–109}$ monomers, and 132–225 and 132–226, respectively, of the two copies of Flt-1_{D2}, together with 476 water molecules.

Structure of $VEGF_{8–109}$ as Seen in the Complex

$VEGF_{8–109}$ is an antiparallel homodimer, covalently linked by two disulfide bridges between Cys-51 and Cys-60. It has a rather unusual shape, with a maximum elongation of about 70 Å and a flat central part that barely spans 15 Å. A segment (residues 16–24) near the N terminus of each subunit forms helix α1, which folds on top of the other monomer in the biologically active dimer. A highly irregular four-stranded β sheet comprising strands β1, β3, β5, and β6 (Muller et al., 1997a) forms the central part of the molecule. Two short strands, β4 and β7, are extensions of β3 and β6, classified separately because of an interruption of the hydrogen bonding pattern. The connection between β1 and β3 contains a short α-helical segment followed by a loop and strand β2, which is hydrogen-bonded to strand β5. This short, three-stranded sheet at the end of the molecule opposite to the cystine knot in combination with helix α1 from the other subunit was identified as VEGF's receptor-binding face (Muller et al., 1997a).

The overall structure of $VEGF_{8–109}$ in complex with Flt-1_{D2} is identical to the previously reported structure of free $VEGF_{8–109}$ (Muller et al., 1997a, 1997b), and no major conformational changes are observed on Flt-1_{D2} binding. The two monomers in the complex have a root-mean-square (rms) deviation of 0.64 Å for 94 Cα atoms, which is comparable to the rms deviation of 0.45–0.80 Å calculated for the four copies of free $VEGF_{8–109}$. The largest differences are observed for loop regions 42–48 and 85–89, which have also been shown to vary in free $VEGF_{8–109}$ (Muller et al., 1997b).

Structure of Bound Flt-1_{D2}

The two copies of Flt-1_{D2} in the complex are very similar to each other (the rms difference between them is 0.4 Å calculated over all 94 Cα positions). As predicted on the basis of sequence alignments (Finnerty et al., 1993), Flt-1_{D2} is a member of the IgSF. It consists of a sandwich formed by two β sheets, one consisting of 5 strands (βa′, βc, βc′, βf, and βg), the other of 3 (βb, βd, and βe) (Figure 2). The strands in the three-stranded sheet are rather short and consist of only 3 or 4 residues. In contrast, the five-stranded sheet is more substantial, and strands βf and βg are 9 and 11 residues long, respectively. The crossover connection between strands βe and βf includes a single helical turn at residues 199–201. A disulfide bond between Cys-158 and Cys-207, connecting the segment immediately following strand βb to strand βf, is buried in the hydrophobic core.

The most unusual feature of Flt-1_{D2} is the conformation of the N-terminal segment preceding strand βa′. Instead of pairing up with neighboring strand βg and forming what is strand βa in more standard IgSF domains, residues 137–143 bulge away from the main body of the protein (Figure 2). This bulge is anchored at its C-terminal end by strand βa′ and at its beginning by the side chain of Phe-135, which is buried in the hydrophobic core (Figure 3A). Because several of the residues in this bulge are in contact with VEGF (below), this bulge might be a consequence of complex formation; thus, the possibility exists that free Flt-1_{D2} adopts a more canonical IgSF conformation.

Four distinct classes of IgSF domains have been characterized, the V, C1, C2, and I sets (Harpaz and Chothia,

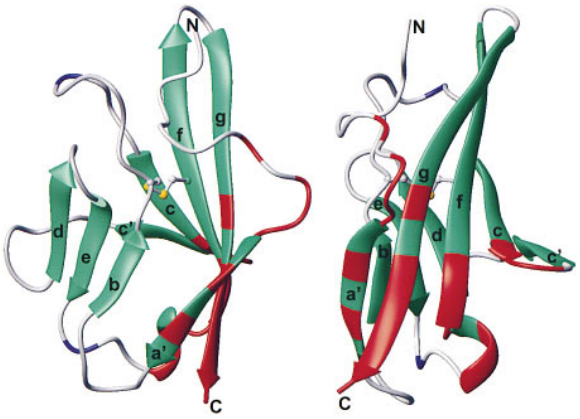

Figure 2. Ribbon Rendering of Flt-1_{D2}, in Two Views Related by a Rotation of Approximately 90° about the Vertical Axis

The termini and the secondary structure elements as defined by the program Procheck (Laskowski et al., 1993) are labeled; β strands are rendered as green arrows, the helical turn as a green ribbon, and the loop regions as gray tubes. The disulfide bond is shown in ball-and-stick rendering, with sulfur atoms colored yellow. The two potential N-linked glycosylation sites at Asn-164 and Asn-196 are colored blue. The VEGF binding site is located on the "bottom" end of the five-stranded sheet; residues in contact with VEGF in the complex are colored red. A segment near the N terminus, which forms strand βa in members of the I set of the immunoglobulin superfamily, bulges away from the core of the domain. This figure was created using the program MOLMOL (Koradi et al., 1996).

1994). The structure shows that Flt-1_{D2} is a distant member of the I set, despite significant differences from canonical I-set structures. Flt-1_{D2} has a strand topology that is similar to that of I-set member telokin (Holden et al., 1992) and can be superimposed on the telokin structure with an rms difference of 1.4 Å (66 Cα atoms within a distance cutoff of 3.0 Å). Of the 20 key positions in the V-frame profile that define the I set (Harpaz and Chothia, 1994), only 14 fulfill the required criteria in Flt-1_{D2}. The other 6 positions all involve residues displayed from the five-stranded sheet. Two differences are found in the so-called "Y-corner" motif, a sequence consisting of residues D-x-G/A/D-x-Y-x-C (Hemmingsen et al., 1994), at the N-terminal end of strand βf. The first aspartic acid is replaced conservatively by Glu-201, and the tyrosine residue by Leu-205. Usually, the tyrosine hydroxyl group forms a hydrogen bond to the carbonyl oxygen of the first residue of the motif. In Flt-1_{D2}, this hydrogen-bonding function is fulfilled instead by Thr-222 from strand βg, which is normally a key hydrophobic residue (Figure 3B). The overall conformation of this region remains very similar to the standard Y-corner motif; thus, this alternative set of residues constitute a variation of this structural feature. Strand βg contains two other sites, which in Flt-1_{D2} are occupied by Tyr-220 and Arg-224 instead of strictly hydrophobic residues. The side chain of Tyr-220 occupies the position taken by strand βa in telokin; therefore, this change may be related to the unusual bulging N-terminal segment of Flt-1_{D2}. Interestingly, Arg-224 has a special function as ligand binding determinant, because its side chain makes intimate charge-mediated hydrogen bonding interactions with VEGF (Figure 3C; see below). Finally, a buried tryptophan residue on strand βc that is strictly conserved among I-set members is leucine in Flt-1_{D2}; the smaller size of the Leu-169 side chain is compensated for by other buried residues nearby.

The VEGF–Flt-1_{D2} Interface

The overall structure of the complex follows the internal approximate two-fold symmetry of the VEGF dimer (Figure 4). However, the differences in crystal packing environment between the two individual molecules do introduce some differences in orientation. Superposition of the entire complex onto itself, rotated around the local two-fold symmetry axis, results in a rather large rms deviation of 1.54 Å for 376 Cα atoms. This difference is accounted for by small rotations of the individual Flt-1_{D2} molecules with respect to the VEGF dimer, pivoted around the interface. The two interfaces themselves are virtually identical, with the exception of two poorly defined residues near the C terminus of Flt-1_{D2}. Excluding these two residues from the calculation, the total surface buried by $VEGF_{8–109}$ on Flt-1_{D2} is 827 $Å^2$ and 817 $Å^2$, respectively, for each of the two copies.

Flt-1_{D2} is in contact with both subunits of the ligand. The region covered on $VEGF_{8–109}$ agrees well with the previously proposed receptor-binding face (Muller et al., 1997a) but includes more of the exposed surface on the "pole" of the molecule than previously suspected (see Figure 5). The contact surface is divided about 65%/35% between the two VEGF subunits. The segments of $VEGF_{8–109}$ in contact with Flt-1_{D2} include residues from the N-terminal helix (16–27), the loop connecting β3 to β4 (61–66) and strand β7 (103–106) of one monomer, as well as residues from strand β2 (46–48) and from strands β5 and β6 together with the connecting turn (79–91) of the other. Flt-1_{D2} faces VEGF with the "bottom" half of its five-stranded sheet (Figure 2), a surface made up of residues from the N-terminal bulge, strand βa′, part of strands βg and βf, the loop connecting strands βc and βc′, and the helical turn connecting strands βe and βf.

Figure 5 shows a space-filling rendering of the surfaces buried in the interface between $VEGF_{8–109}$ and Flt-1_{D2}. The interface is dominated by hydrophobic contacts, which make up almost 70% of the total buried surface. Altogether, of 21 ligand and 26 receptor residues contributing to the interface, 9 are leucine or isoleucine residues, accounting for 24% of the total buried surface. It is noteworthy that both the surface of the ligand and the surface of the receptor are rather flat and lack a predominant knob-into-hole interaction. The only direct polar interaction is a bidentate set of charge-mediated hydrogen bonds between the side chains of Arg-224 of Flt-1_{D2} and Asp-63 of VEGF (Figure 3C). In addition, 14 buried solvent molecules are found in the interface, 7 of which bridge between the ligand and the receptor (see Figure 3C). Three water molecules are trapped in a cavity near the center of the interface, formed by Asn-62, Tyr-21, and Lys-48 of VEGF and Ile-202, Gly-203, Thr-222, and His-223 of Flt-1_{D2}.

Discussion

Domain 2 of Flt-1 Is Sufficient for Tight VEGF Binding

Dimerized forms of KDR bind about 100-fold more tightly than their corresponding monomeric forms (Fuh et al.,

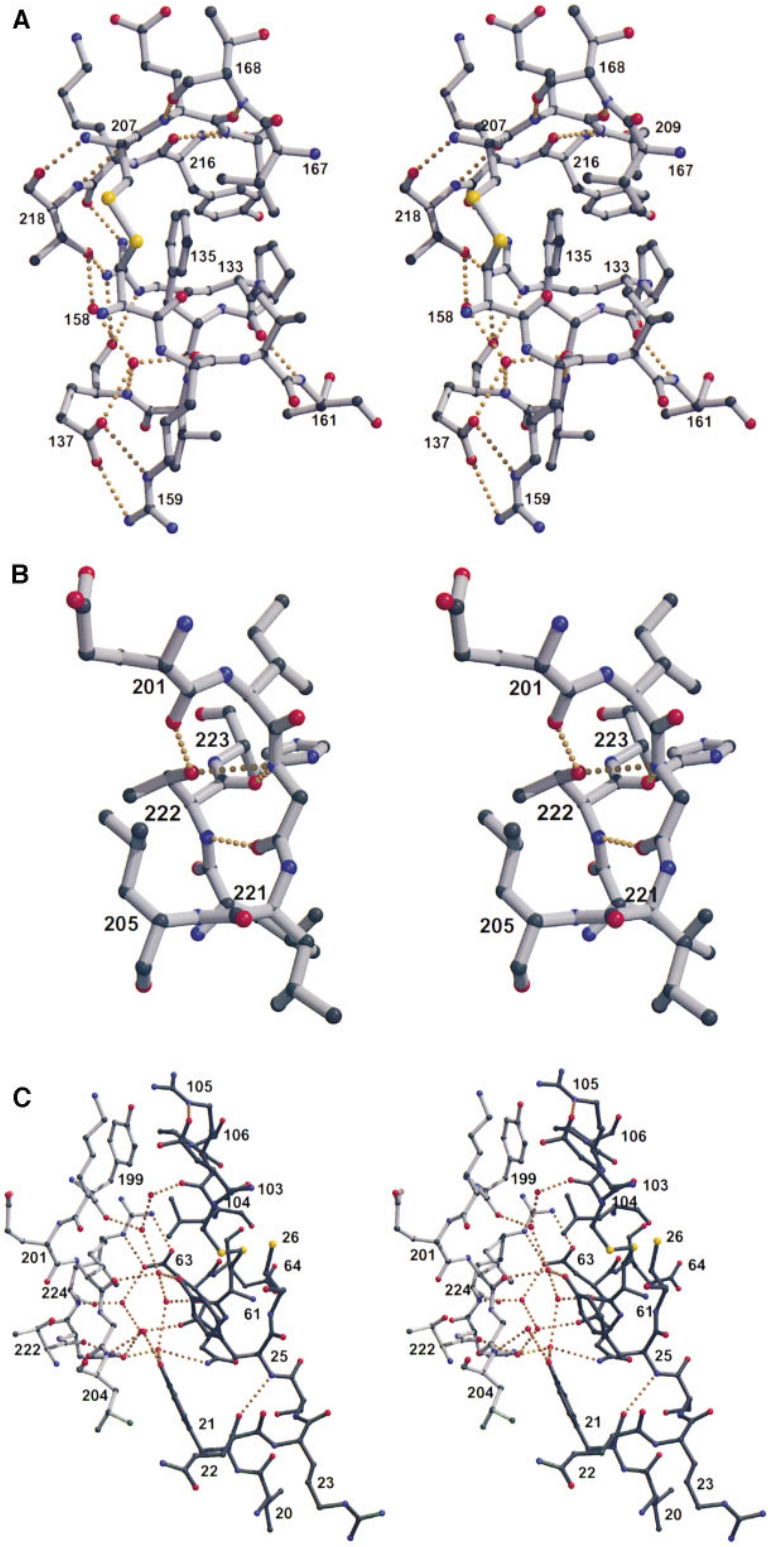

Figure 3. Stereo Views in Ball-and-Stick Rendering of Structural Details

Hydrogen bonds are shown as dotted lines; oxygen atoms are colored red, nitrogens dark blue, and carbons gray. This figure was generated using the programs MOLSCRIPT (Kraulis, 1991) and RASTER3D (Merrit and Murphy, 1994).

(A) The environment of Phe-135 of Flt-1.

(B) The region in Flt-1 corresponding to the "Y corner" found in most Greek key barrel proteins.

(C) A region of the interface between VEGF (in dark gray) and Flt-1 (in light gray) around the interaction between Asp-63 and Arg-224, showing a chain of water molecules in the interface.

submitted), while dimerized forms of Flt-1 bind only 2-fold more tightly. The reason for the difference in avidity could be that receptor–receptor interactions in dimerized receptors would not add significantly to the binding energy of monomeric Flt-1 constructs binding tightly to both poles of VEGF. Alternatively, the high affinity of monomeric Flt-1 for VEGF could have reached the sensitivity limit of the assay. At any rate, monomeric Flt-1 binds VEGF about 100-fold more tightly than monomeric KDR.

Our deletion analysis of Flt-1 shows that domains 2–3 are sufficient for binding $VEGF_{8–109}$ with near wild-type affinity. Similar results were found for deletions in KDR (Fuh et al., submitted). Further deletion of domain 3 of

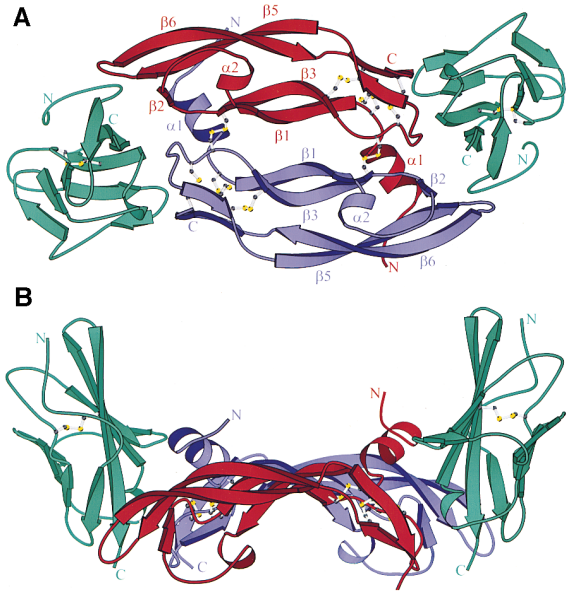

Figure 4. Ribbon Representation of the Complex Between $VEGF_{8–109}$ and $Flt\text{-}1_{D2}$

The two monomers of $VEGF_{8–109}$ are shown in red and blue, respectively; the two copies of $Flt\text{-}1_{D2}$ in green. The secondary structure elements of $VEGF_{8–109}$ as well as all terminal residues are labeled. (A) "Bottom" view, looking up from the membrane; (B) side view, with the membrane below. Ribbon representation generated using the program MOLSCRIPT (Kraulis, 1991).

Flt-1, however, only causes a 20-fold decrease in affinity, compared to a larger than 1000-fold decrease for KDR. Thus, the relative importance of domain 3 is different for Flt-1 and KDR. $Flt\text{-}1_{D2}$ produced from E. coli binds $VEGF_{8–109}$ with an affinity similar to that of a glycosylated construct of domains 1–2. This is consistent with previous studies showing that glycosylation of Flt-1 is not important for binding (Barleon et al., 1997). However, these results contradict reports suggesting that domain 2 by itself is not sufficient for binding (Davis-Smyth, 1996; Barleon et al., 1997; Cunningham et al., 1997). The discrepancy is likely due to the choice of domain boundaries. This can now be rationalized, because the structure shows that the previous deletions either cut into the last β strand of the second domain or had extra residues that presumably destabilize the overall folding. The importance of domain 2 for biological function is demonstrated by the observation that it contains epitopes for the three neutralizing antibodies and that it can inhibit the activity of $VEGF_{165}$ in a human endothelial cell proliferation assay.

Comparison with the KDR Binding Site Deduced from Mutagenesis Data

A comprehensive mutagenesis study of VEGF has enabled us to identify its receptor-binding determinants for KDR and to define its receptor-binding face (Muller et al., 1997a). Of the 7 VEGF residues that were found to be of moderate to great importance for tight binding to KDR, 5 are buried in the interface with $Flt\text{-}1_{D2}$ in the structure of the complex (Figure 5), suggesting that the binding sites for KDR and Flt-1 are very similar. The remaining two binding determinants for KDR are Glu-64 and Ile-43, for which alanine substitution resulted in 110- and 20-fold decreased affinity, respectively. These residues are located just outside the contact region with $Flt\text{-}1_{D2}$ (see Figure 5) and form part of a groove that connects the "pole" to the "bottom" face of VEGF. The observation that the C-terminal segment of $Flt\text{-}1_{D2}$ ends in the immediate vicinity of this groove (Figure 6A) suggests that in the native complex, these residues may contact the third domain of the receptor.

Location of Domains 1 and 3 in the Native Complex

The second domain of Flt-1 uses the C-terminal half of its five-stranded sheet to bind to the pole of the flat and elongated VEGF dimer. This orientation places the N terminus of $Flt\text{-}1_{D2}$ at a distance of 28 Å from $VEGF_{8–109}$, pointing away from the ligand (see Figure 4). Moreover, our domain deletion studies show that deletion of domain 1 only affects binding affinity by two-fold or less. Therefore, we believe it is unlikely that the first domain of Flt-1 interacts directly with the ligand in the native

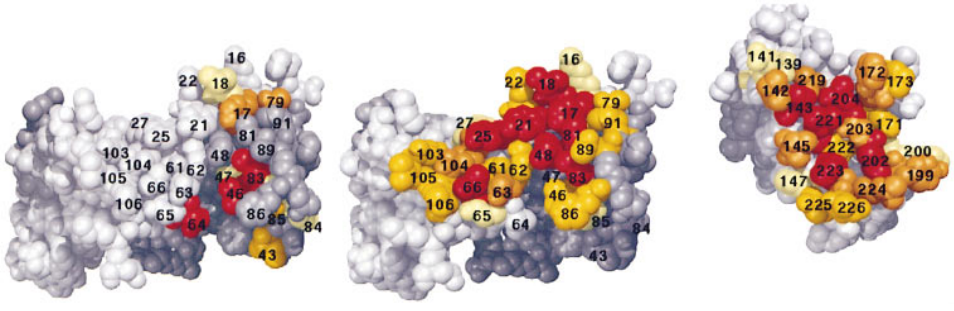

Figure 5. Space-Filling Rendering of $VEGF_{8–109}$ and $Flt\text{-}1_{D2}$, in "Open Book" View

(Left) Functional map of the KDR binding site on the receptor binding domain of VEGF (Muller et al., 1997a). Binding determinants are color-coded based on the magnitude of the decrease in binding upon alanine substitution (dark red, >100-fold; orange, 50- to 100-fold; yellow, 10- to 50-fold; light yellow, 3- to 10-fold).

(Center and Right) Buried surface between $VEGF_{8–109}$ (center) and $Flt\text{-}1_{D2}$ (right). Contact residues are color-coded in different shades of red, reflecting the percentage of accessible surface buried in the interface (dark red, 75%–100%; orange, 50%–75%; yellow, 25%–50%; light yellow, 0%–25%). The two VEGF images have been adjusted to create a wall-eyed stereo view of the surface; note the groove between residues 64 and 43. Model generated using the program CONIC (Huang et al., 1991).

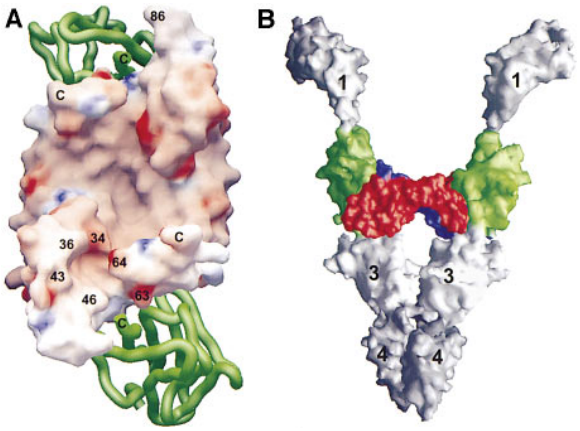

Figure 6. Location of Other Domains of Flt-1

(A) Surface rendering of $VEGF_{8–109}$ with the contact regions of Flt-1_{D2} in tube representation, generated using the program GRASP (Nicholls et al., 1993) and color-coded for electrostatic potential. Blue and red indicate positively and negatively charged patches on the surface of $VEGF_{8–109}$, respectively; selected VEGF residues are labeled. The C terminus of Flt-1_{D2} reaches toward a groove between Glu-64 and Ile-43. Glu-64 is an important binding determinant of VEGF for binding to Flt-1 (Keyt et al., 1996b), and both of these residues are important for high-affinity binding of VEGF to KDR (Muller et al., 1997a).

(B) Model of a complex between $VEGF_{8–109}$ and domains 1–4 of Flt-1. The two VEGF subunits are colored red and blue, respectively, domain 2 of Flt-1 is in green, and the other domains of Flt-1 are in different shades of gray.

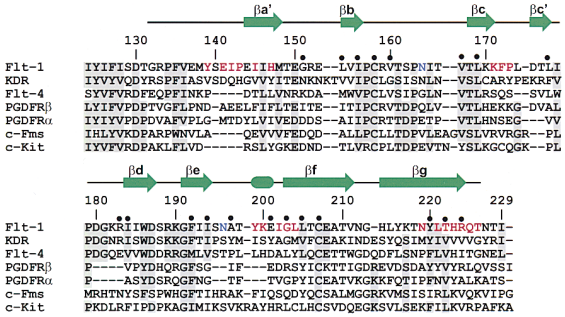

Figure 7. Sequence Alignment of Domain 2 of the Members of the PDGF Receptor Family

Secondary structure elements observed for Flt-1_{D2} are shown and labeled as in Figure 2, and key I-set positions are marked by closed circles. Homologous residues are shaded, Flt-1 residues in contact with VEGF are shown in red, and the two potential N-linked glycosylation sites of Flt-1_{D2} are in blue. Human sequences were taken from the SwissProt Data Bank (accession numbers P17948, P35968, P35916, P09619, P16234, P07333, and P10721).

complex. If this is true, a possible function for this domain might be that in the absence of ligand it shields the hydrophobic surface of domain 2, and then is displaced by VEGF upon complex formation.

Compared to domain 2 alone, a construct of domains 2 and 3 binds VEGF about 20-fold tighter. This observation, combined with the analysis of the mutagenesis data in light of our crystal structure, strongly suggests that domain 3 is involved in direct contacts with the ligand. In the structure of the complex, the C-terminal three residues of Flt-1_{D2} are disordered, but the visible C-terminal end extends toward a 6.5 Å wide groove between the monomers, which connects the pole of VEGF to its membrane-facing side (Figure 6A). The walls of this groove are formed by the side chains of Asp-63 and Glu-64 on one side, and Ile-43, Ile-46, and Tyr-36 on the other, while the bottom is made of Asp-34 and Ser-30. The groove appears barely wide enough to accommodate a polypeptide chain, but the residues forming the walls reside on flexible regions of $VEGF_{8–109}$ in its free state (Muller et al., 1997b). Furthermore, the side chains of Phe-36 and Ile-46 adopt different conformations in the two copies of $VEGF_{8–109}$ in our complex, suggesting an additional mechanism for widening the groove. Based on these observations, we suggest that in the native complex the linker between domains 2 and 3 may occupy the groove, positioning the third domain in contact with the "bottom" face of VEGF. (We believe the reason for the disordered C terminus of our construct may be that electrostatic repulsion between the artificial C terminus and Glu-64 and Asp-34 of VEGF prevents the chain from entering the groove.)

Using the structures of Flt-1_{D2} and telokin (Holden et al., 1992) as templates, we built models of the individual domains 1, 3, and 4 of Flt-1. We then constructed a dimeric model of the receptor-binding domain of VEGF in complex with domains 1–4 of Flt-1 (Figure 6B), based on the assumptions described above. In this model, domain 1 points away from the ligand, the domain 2–3 linker occupies the groove in VEGF, and domain 3 is in contact with its "bottom" face. The likely orientation of the two copies of domain 3 places their C-terminal ends in close proximity, suggesting direct receptor–receptor contacts between domains 4 (Figure 6B). This function of domain 4 agrees with previous proposals that it may be involved in receptor dimerization of Flt-1 (Barleon et al., 1997).

Implications for Other PDGF Receptor Family Members

Sequence alignment of the members of the PDGF receptor family reveals that their first four domains have many of the key I-set residues, suggesting that they all belong to the I set of the IgSF. Furthermore, many of the unique features of Flt-1_{D2} are conserved in the second domain of the other members, suggesting that they share similar structural characteristics distinct from the other domains of these receptors (Figure 7). For example, the characteristic core tryptophan residue of strand βc is always a leucine in the second domain. Residue Phe-135 of Flt-1_{D2}, anchoring the N-terminal bulge to the core of the domain, is conserved as phenylalanine (tryptophan in Fms) in domain 2 of all receptors of the PDGF family, suggesting that the distinctive bulge of Flt-1_{D2} may be present in some of the other members as well. In Flt-1_{D2}, strand βb comprises only three residues and is terminated by a Pro-Cys motif, which is conserved in all second domains except that of Kit. The βe strand contains a strictly conserved Gly-191, leaving room to accommodate the side chain of Trp-186, which is conserved as an aromatic residue in all members except Kit. Finally, the linker region between domains 1 and 2

has a rather well-conserved consensus sequence Y-V/L/I-F/Y-I/V-x-D.

Domain deletion studies on the PDGF receptor (Mahadevan et al., 1995), on Kit (Blechman et al., 1995; Lemmon et al., 1997), and on Flt-1 (Davis-Smyth et al., 1996; Barleon et al., 1997) have previously indicated that domains 2 and 3 carry ligand-binding determinants of these receptors. We have demonstrated that these same two domains of KDR (Fuh et al., submitted) and Flt-1 are necessary and sufficient for native affinity. For Flt-1 (Barleon et al., 1997) and Kit (Blechman et al., 1995), ligand-induced cross-linking of receptors was only observed for constructs containing at least the first four domains, suggesting that in the complex the two copies of domain 4 are close together. Taken together with our crystal structure, these data and the sequence similarities discussed above suggest a common structural scaffold used in the same functional manner. Thus, the receptors of the PDGF family may all use domains 2 and 3 for ligand binding and domain 4 for direct receptor–receptor contacts, in a way generally analogous to our model of $VEGF_{8-109}$ in complex with domains 1–4 of Flt-1.

Experimental Procedures

Production of Deletion Variants and of Flt-1 Domain 2

Transient expression in 293 cells of the IgG fusions of Flt-1 variants and production of the monomers of Flt-1 domains 1–7 and 1–3 are described elsewhere (Fuh et al., submitted). Constructs containing Flt-1 domains 1–5, 1–4, 1–3, 1–2, and 2–3 correspond to amino acids 1–558, 1–431, 1–339, 1–229, and 1–339 with 27–131 deleted, respectively. N-terminal analysis of the secreted protein, Flt-1 domains 1–7, shows that residues 1–26 constitute the signal sequence. For expression of domain 2 alone, residues 129–229 of Flt-1 were constructed in a phagemid vector under the control of an alkaline phosphatase promoter and stII secretion signal.

Binding Assays

Receptor binding assays using [^{125}I]$VEGF_{165}$ (ICN, DuPont) and monoclonal antibody binding assays were done as described elsewhere (Fuh et al., submitted). Briefly, receptor-IgG fusions or monomers were incubated with [^{125}I]$VEGF_{165}$ and increasing concentrations of $VEGF_{8-109}$ for 18 hr at room temperature in 100 μl of binding buffer containing 0.5% bovine serum albumin, 0.05% Tween 20, 0.15 M NaCl, and 20 mM Tris–HCl (pH 7.5). The mixture was transferred to a 96-well plate coated with anti-Fc antibody for Flt-1-IgG assays or MAFL3 for Flt-1 monomer assays and allowed to equilibrate for 15 min before washing and counting the plate. For binding assays with E. coli–expressed domain 2, biotinylated $VEGF_{8-109}$ was used. Dilutions of purified Flt-1_{D2} were incubated with 0.5 nM of biotinylated $VEGF_{8-109}$ for 2 hr on a 96-well plate coated with an anti-VEGF monoclonal antibody that competes with Flt-1_{D2} binding before adding horseradish peroxidase–conjugated Streptavidin (Jackson ImmunoResearch Lab, Inc., West Grove, PA).

[^{3}H]Thymidine Incorporation Assay

For assays with human umbilical vein endothelial cells (purchased from Cell System, Kirkland, WA), cells were seeded in 96-well plates (2000 cells per well) and fasted in DMEM F12 media with 1% DFBS for 24 hr. $VEGF_{165}$ (0.2 nM) together with increasing concentrations of the Flt-1 variants was added in fresh fasting media, incubated for 18 hr, and pulsed with [^{3}H]thymidine (0.5 μCi/well) for 24 hr, after which the cells were harvested and counted.

Refolding and Purification

$VEGF_{8-109}$ was expressed, refolded, and purified as described (Christinger et al., 1996). A construct comprising residues 129–229 of Flt-1, corresponding to the second IgSF domain, was expressed as an insoluble protein in E. coli. Inclusion bodies were isolated by passing homogenized cells in 20 mM Tris–HCl (pH 7.5), 5 mM EDTA through a French pressure cell and centrifuging the homogenate for 15 min at 4000 × g. The inclusion bodies were resuspended and the centrifugation repeated. The pellet containing primarily Flt-1_{D2} was dissolved in 6 M urea, 20 mM Tris–HCl (pH 7.5), and stirred for 1–2 hr in 10 mM DTT. The protein was refolded by diluting the above solution in 6 M urea to 0.05 mg/ml and dialyzing overnight against 2 M urea, 20 mM Tris–HCl (pH 8.0), 1 mM cysteine. The resulting solution was further dialyzed against Tris–HCl (pH 8.0) for another 24 hr.

Refolded Flt-1_{D2} was purified to homogeneity in consecutive steps of hydrophobic interaction (Alkyl-Sepharose, Pharmacia) and size exclusion chromatography (S-100, Pharmacia). The purity of the protein was assessed by SDS–PAGE and mass spectrometry. Final yields from refolding were about 10 mg per 50 g of cell paste, or about 20% of total Flt-1_{D2}. Purified Flt-1_{D2} was mixed in a 2.1:1 molar ratio with $VEGF_{8-109}$. The resulting complex was purified by gel filtration chromatography (S-200, Pharmacia) and concentrated by ultra filtration to 7 mg/ml. The composition of the complex was confirmed by size exclusion chromatography and reverse-phase HPLC (Vydac, 214 nm).

Crystallization and Data Collection

Crystals were grown by vapor diffusion at room temperature using the hanging drop method. Crystallization buffer containing 30% PEG-4000, 0.2 M ammonium sulfate, 0.02% NaN_3, and 0.15 M Tris–HCl at pH 8.5 was mixed in equal volume with protein solution (7 mg/ml, 20 mM Tris–HCl [pH 7.5]). Two different crystal forms were found that appeared occasionally in the same drops. Both crystal forms belonged to space group C2 with cell dimensions of a = 81.44 Å, b = 71.13 Å, c = 77.86 Å, β = 105.28° (form A), and a = 124.31 Å, b = 67.01 Å, c = 120.84 Å, β = 118.15° (form B), respectively. These crystal forms contained 1 and 2 complexes, respectively, in the asymmetric unit.

Crystals were soaked in artificial mother liquor (30% PEG-4000, 0.2 M ammonium sulfate, 0.15 M Tris–HCl [pH 8.5]), then dipped in artificial mother liquor brought to 10% glycerol and flash-frozen in liquid nitrogen. A 1.7 Å data set from a form A crystal was collected on an ADSC 1K CCD detector at the Cornell High Energy Synchrotron Source on beam line A1, λ = 0.908 Å. For form B, data to 2.7 Å resolution were collected on a MAR-Research imaging plate system using a Rigaku rotating anode generator with mirror-focused CuKα radiation. The data sets were reduced using programs DENZO and SCALEPACK (Otwinowski, 1993) (Table 2).

Structure Determination and Refinement

The structure was determined by molecular replacement and 6-fold noncrystallographic symmetry averaging across the two crystal forms. Using the program AMoRe (CCP4, 1994) and the high resolution structure of the free $VEGF_{8-109}$ dimer (Muller et al., 1997b) as a search model, clear solutions were found for one dimer in the form A cell and two independent dimers in the form B cell. The initial R values for all data between 12 and 4 Å were 48.2% and 49.2% for the A and B crystal forms, respectively. Attempts to place models of Flt-1_{D2} failed.

To identify the position of the Flt-1_{D2} molecules, a mask with a radius of 30 Å was created around the $VEGF_{8-109}$ molecules in the A cell and then transferred to the B cell. After overlap removal with program NCSMASK (CCP4, 1994) in both crystal forms, the edited mask was used for solvent flattening and 6-fold cross-crystal averaging with program DMMULTI (CCP4, 1994), using the symmetry operators relating the $VEGF_{8-109}$ molecules to each other. The resulting electron density was partially interpretable for 5 of the 6 expected Flt-1_{D2} molecules and allowed building of about 60% of the known sequence. Symmetry operators relating the resulting fragments were optimized by rigid body refinement using the program X-PLOR (Brünger et al., 1987), and the refined positions were used to improve the mask.

The refined symmetry operators, improved mask, and phase information from the $VEGF_{8-109}$ molecules and the partial model of Flt-1_{D2} were used in a subsequent averaging procedure, resulting in greatly improved electron density maps. Subsequent model building and

refinement were done in crystal form A, using the programs O (Jones et al., 1991), X-PLOR (Brünger et al., 1987), and REFMAC (CCP4, 1994). A random set of 2275 reflections was sequestered and used to monitor the free R value (Brünger, 1992). Alternate cycles of refinement and model building, accompanied by addition of water molecules, and inclusion of a solvent mask (k = 0.39 e/Å^3, B = 65 Å^2), resulted in the final model with R_{free} = 26.1% and good stereochemistry (see Table 2). Structural comparisons were done using the program O, with a distance cutoff of 3.8 Å unless otherwise indicated.

Model Building

The 20 I-set domain fingerprint residues were identified in the sequences of domains 1, 3, and 4 of Flt-1, and models of these domains were built using the structures of Flt-1_{D2} and telokin as templates. Domains 1 and 2 were connected through an eight-residue linker. Domain 3 was built with a bulge in its N-terminal segment like that observed in domain 2; this bulge was placed in the groove of VEGF connecting its pole to its "bottom" face. This arrangement positioned the C-terminal ends of the two symmetry-related copies of domain 3 close to each other. Domain 4 was placed in intimate contact with its symmetry mate, using an eight-residue link from domain 3.

Acknowledgments

We thank Han Chen for fermentation runs, Beth Gillece-Castro and Jim Bourell for mass spectrometry data, the staff at CHESS for help with beam line A1, Trissa Elkins and Mike Randal for help with data collection, Brian Cunningham and Bing Li for discussions of their mutagenesis data, and Len Presta for his model of Flt-1_{D2} and for advice on IgSF domain classification.

Received September 15, 1997; revised October 16, 1997.

References

Barleon, B., Totzke, F., Herzog, C., Blanke, S., Kremmer, E., Siemeister, G., Marmé, D., and Martiny-Baron, G. (1997). Mapping of the sites for ligand binding and receptor dimerization at the extracellular domain of the vascular endothelial growth factor receptor flt-1. J. Biol. Chem. *272*, 10382–10388.

Blechman, J.M., Lev, S., Barg, J., Eisenstein, M., Vaks, B., Vogel, Z., Givol, D., and Yarden, Y. (1995). The fourth immunoglobulin domain of the stem cell factor receptor couples ligand binding to signal transduction. Cell *80*, 103–113.

Brünger, A.T. (1992). Free R value: a novel statistical quantity for assessing the accuracy of crystal structures. Nature *355*, 472–475.

Brünger, A.T., Kuriyan, J., and Karplus, M. (1987). Crystallographic R factor refinement by molecular dynamics. Science *235*, 458–460.

Carmeliet, P., Ferreira, V., Breier, G., Pollefeyt, S., Kieckens, L., Gertsenstein, M., Fahrig, M., Vandenhoeck, A., Harpal, K., Eberhardt, C., et al. (1996). Abnormal blood vessel development and lethality in embryos lacking a single VEGF allele. Nature *380*, 435–439.

CCP4. (1994). The CCP4 suite: programs for protein crystallography. Acta Crystallogr. *D50*, 760–763.

Christinger, H.W., Muller, Y.A., Berleau, L., Keyt, B.A., Cunningham, B.C., Ferrara, N., and De Vos, A.M. (1996). Crystallization of the receptor binding domain of vascular endothelial growth factor. Prot. Struct. Funct. Genet. *26*, 353–357.

Cunningham, S.A., Stephan, C.C., Arrate, M.P., Ayer, K.G., and Brock, T.A. (1997). Identification of the extracellular domains of flt-1 that mediate ligand interactions. Biochem. Biophys. Res. Commun. *231*, 596–599.

Davis-Smyth, T., Chen, H., Park, J., Presta, L.G., and Ferrara, N. (1996). The second immunoglubulin-like domain of the VEGF tyrosine kinase receptor Flt-1 determines ligand binding and may initiate a signal transduction cascade. EMBO J. *15*, 4919–4927.

Dvorak, H.F., Brown, L.F., Detmar, M., and Dvorak, A.M. (1995). Vascular permeability factor/vascular endothelial growth factor, microvascular hyperpermeability, and angiogenesis. Am. J. Pathol. *146*, 1029–1039.

Ferrara, N. (1995). The role of vascular endothelial growth factor in pathological angiogenesis. Breast Cancer Res. Treat. *36*, 127–137.

Ferrara, N., Carver-Moore, K., Chen, H., Dowd, M., Lu, L., O'Shea, K.S., Powell-Braxton, L., Hillan, K.J., and Moore, M.W. (1996). Heterozygous embryonic lethality induced by targeted inactivation of the VEGF gene. Nature *380*, 439–442.

Finnerty, H., Kelleher, K., Morris, G.E., Bean, K., Merberg, D.M., Kriz, R., Morris, J.C., Sookdeo, H., Turner, K.J., and Wood, C.R. (1993). Molecular cloning of murine FLT and FLT4. Oncogene *8*, 2293–2298.

Fong, G.-H., Rossant, J., Gertsenstein, M., and Beritman, M.L. (1995). Role of the flt-1 receptor tyrosine kinase in regulating the assembly of vascular endothelium. Nature *376*, 66–70.

Harpaz, Y., and Chothia, C. (1994). Many of the immunoglobulin superfamily domains in cell adhesion molecules and surface receptors belong to a new structural set which is close to that containing variable domains. J. Mol. Biol. *238*, 528–539.

Hemmingsen, J.M., Genert, K.M., Richardson, J.S., and Richardson, D.C. (1994). The tyrosine corner: a feature of most greek key β-barrel proteins. Prot. Sci. *3*, 1927–1937.

Holden, H.M., Ito, M., Hartshorne, D.J., and Rayment, I. (1992). X-ray structure determination of telokin, the C-terminal domain of myosin light chain kinase at 2.8 Å resolution. J. Mol. Biol. *227*, 840–851.

Houck, K.A., Ferrara, N., Winer, J., Cachianes, G., Li, B., and Leung, D.W. (1991). The vascular endothelial growth factor family: identification of a fourth molecular species and characterization of alternative splicing of RNA. Mol. Endocrinol. *5*, 1806–1814.

Huang, C.C., Pettersen, E.F., Klein, T.E., Ferrin, T.E., and Langridge, R. (1991). Conic: a fast renderer for space-filling molecules with shadows. J. Mol. Graph. *9*, 230–236.

Jones, T.A., Zhou, J.-Y., Cowan, S.W., and Kjelgaard, M. (1991). Improved methods for building protein models in electron density maps and the location of errors in these models. Acta Crystallogr. *A47*, 110–119.

Keyt, B.A., Berleau, L.T., Nguyen, H.V., Chen, H., Heinsohn, H., Vandlen, R., and Ferrara, N. (1996a). The carboxy-terminal domain (111–165) of vascular endothelial growth factor is critical for its mitogenic potency. J. Biol. Chem. *271*, 7788–7795.

Keyt, B.A., Nguyen, H.V., Berleau, L.T., Duarte, C.M., Park, J., Chen, H., and Ferrara, N. (1996b). Identification of vascular endothelial growth factor determinants for binding KDR and flt-1 receptors. J. Biol. Chem. *271*, 5638–5646.

Kim, J.K., Li, B., Winer, J., Armanini, M., Gillet, N., Phillips, H.S., and Ferrara, N. (1993). Inhibition of vascular endothelial growth factor-induced angiogenesis suppresses tumour growth in vivo. Nature *362*, 841–844.

Koradi, R., Billeter, M., and Wüthrich, K. (1996). MOLMOL: a program for display and analysis of macromolecular structures. J. Mol. Graph. *14*, 51–55.

Kraulis, P.J. (1991). MOLSCRIPT: a program to produce both detailed and schematic plots of protein structure. J. Appl. Crystallogr. *24*, 946–950.

Laskowski, R.A., MacArthur, M.W., Moss, D.S., and Thornton, J.M. (1993). Procheck: a program to check the stereochemical quality of protein structures. J. Appl. Crystallogr. *26*, 283–291.

Lemmon, B.A., Pinchasi, D., Zhou, M., Lax, I., and Schlessinger, J. (1997). Kit receptor dimerization is driven by bivalent binding of stem cell factor. J. Biol. Chem. *272*, 6311–6317.

Mahadevan, D., Yu, J.-C., Saldanha, J.W., Thanki, N., McPhie, P., Uren, A., LaRochelle, W.J., and Heidaran, M.A. (1995). Structural role of the extracellular domain-1 of α-platelet-derived growth factor (PDGF) receptor for PDGF-AA and PDGF-BB binding. J. Biol. Chem. *270*, 27595–27600.

Merrit, E.A., and Murphy, M.E.P. (1994). Raster3D version 2.0, a program for photorealistic molecular graphics. Acta Crystallogr. *D53*, 240–255.

Millauer, B., Wizigmann-Voos, S., Schnurch, H., Martinez, R., Moller,

N.P., Risau, W., and Ullrich, A. (1993). High affinity VEGF binding and developmental expression suggest Flk-1 as a major regulator of vasculogenesis and angiogenesis. Cell *72*, 835–846.

Muller, Y.A., Li, B., Christinger, H.W., Wells, J.A., Cunningham, B.C., and De Vos, A.M. (1997a). Vascular endothelial growth factor: crystal structure and functional mapping of the kinase domain receptor binding site. Proc. Natl. Acad. Sci. USA *94*, 7192–7197.

Muller, Y.A., Christinger, H.W., Keyt, B.A., and De Vos, A.M. (1997b). The crystal structure of vascular endothelial growth factor (VEGF) refined to 1.93 Å resolution: multiple copy flexibility and receptor binding. Structure *5*, 1325–1338.

Nicholls, A., Bharadwaj, R., and Honig, B. (1993). GRASP: graphical representation and analysis of surface properties. Biophys. J. *64*, 166–170.

Otwinowski, Z. (1993). DENZO. In Data Collection and Processing, L. Sawyer, N. Isaacs, and S. Bailey, eds. (Warrington, UK: SERC Daresbury Laboratory), pp. 56–62.

Peters, K.G., De Vries, C., and Williams, L.T. (1993). Vascular endothelial growth factor receptor expression during embryogenesis and tissue repair suggests a role in endothelial differentiation and blood vessel growth. Proc. Natl. Acad. Sci. USA *90*, 8915–8919.

Shalaby, F., Rossant, J., Yamaguchi, R.P., Gertsenstein, M., Wu, X.-F., Breitman, M.L., and Schuh, A.C. (1995). Failure of blood-island formation and vasculogenesis in flk-1 deficient mice. Nature *376*, 62–66.

Sun, P.D., and Davies, D.R. (1995). The cystine-knot growth-factor superfamily. Annu. Rev. Biophys. Biomol. Struct. *24*, 269–291.

Tischer, E., Mitchell, R., Hartman, T., Silva, M., Gospodarowicz, D., Fiddes, J.C., and Abraham, J.A. (1991). The human gene for vascular endothelial growth factor. Multiple protein forms are encoded through alternative splicing of RNA. J. Biol. Chem. *266*, 11947–11954.

Van der Greer, P., and Hunter, T. (1994). Receptor protein-tyrosine kinases and their signal transduction pathways. Annu. Rev. Cell Biol. *10*, 251–337.

Vaisman, N., Gospodarowicz, D., and Neufeld, G. (1990). Characterization of the receptors for vascular endothelial growth factor. J. Biol. Chem. *265*, 19461–19466.

Williams, A.F., and Barclay, A.N. (1988). The immunoglobulin superfamily—domains for cell surface recognition. Annu. Rev. Immunol. *6*, 381–405.

Protein Data Bank Accession Codes

The coordinates for $VEGF_{8-109}$ in complex with $Flt\text{-}1_{D2}$ have been deposited in the Brookhaven Protein Data Bank under the code 1flt. However, these coordinates will not be released until October 1998.